

A Spherical Crystal Imager for OMEGA EP

Introduction

The unique capabilities of a crystal imaging system using spherically bent Bragg crystals are a narrow spectral width [$\lambda/\Delta\lambda > 1000$, (Ref. 1)], a high throughput (up to 100-fold improvement over pinhole imaging because of the larger solid angle), and a potentially high spatial resolution [$< 2 \mu\text{m}$, (Ref. 2)]. Unlike a pinhole imager, a crystal imaging setup used in backlighting mode is insensitive to spatial nonuniformities in the backlighter intensity distribution because of its limited depth of field.³ The major drawback of crystal imaging is the cost of the crystals and the complexity of the alignment. Crystal imaging has been frequently used on small- to medium-scale facilities, where the target chamber is vented between shots and direct operator access to the target chamber makes the alignment relatively easy.^{1,2,4–7} On larger-scale facilities such as OMEGA EP,^{8,9} where the target chamber stays at vacuum between shots, fully remote alignment of the crystal imager is required; consequently, only a very limited number of setups can be found in the literature.^{3,10}

Experimental Setup

A crystal imaging system that can be remotely aligned and operated has been implemented on OMEGA EP (Fig. 129.39). In the first set of experiments this spherical crystal imaging (SCI) system used a quartz crystal, cut along the 2131 (211) planes for a $2d$ spacing of 0.3082 nm, to image the Cu K_{α} lines at ~ 8 keV. The Bragg angle of the quartz crystal for the Cu K_{α} is 88.7° , very close to normal incidence. The 25-mm-diam, $\sim 150\text{-}\mu\text{m}$ -thick crystal was mounted by means of optical contact on a spherically shaped fused-silica substrate with a curvature radius of $R = 500$ mm. This curvature corresponds to a focal length of $f = R/2 = 250$ mm. The spherically bent crystal was fabricated by the Photonics Products Group, Inc. (PPGI).¹¹ The crystal is placed at a distance of 276 mm from the target, and the image is recorded on an image plate¹² located ~ 2.4 m from the target, resulting in a total magnification of ~ 10 .

The SCI system uses two opposing ten-inch manipulators (TIM's) in its shot configuration, one housing the crystal and the other the image-plate detector. The TIM on OMEGA EP

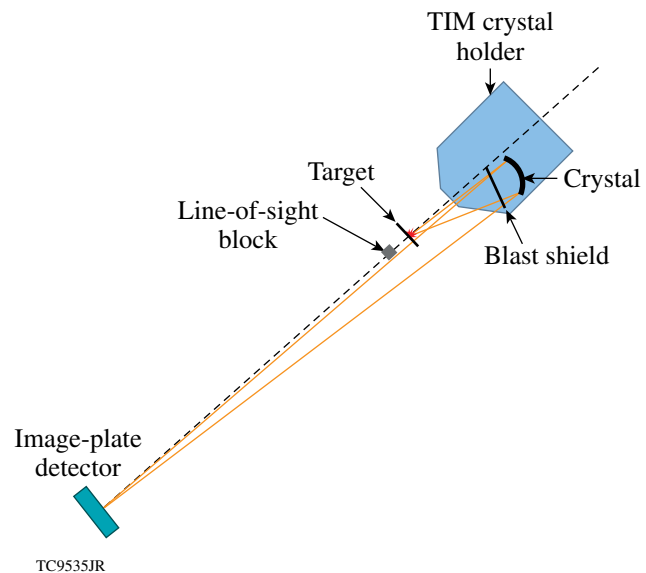


Figure 129.39

Schematic of the spherical crystal imager hardware in shot mode. One ten-inch manipulator (TIM) houses the crystal holder and another houses the image-plate detector. Both TIM's are on a common centerline indicated by the dashed line. A blast shield is placed in front of the spherically bent crystal, which images the target onto the detector. A direct line-of-sight tungsten block is placed opposite the crystal mount beyond the target to protect the detector from x-ray background emitted by the target.

is a fully remote controllable three-axis diagnostic insertion system with an air lock, which allows the insertion of diagnostic modules of up to 25 cm in diameter and 50 kg of weight into the target chamber, without breaking vacuum.

The crystal is mounted on a motorized tip–tilt stage (New Focus 8817-V with PICO motor drive¹³) that sits on a TIM-mounted frame [Fig. 129.40(a)] and is inserted close to the target. A removable blast shield is placed in front of the crystal to protect it from debris. Because of the relatively high energy of the Cu K_{α} , the material and thickness of the blast shield are not critical even though the x rays must pass it twice. A blast shield of 10 to 20 μm of Al foil or 25 μm of Mylar coated with > 100 nm of Al to prevent the scattered laser light from hitting

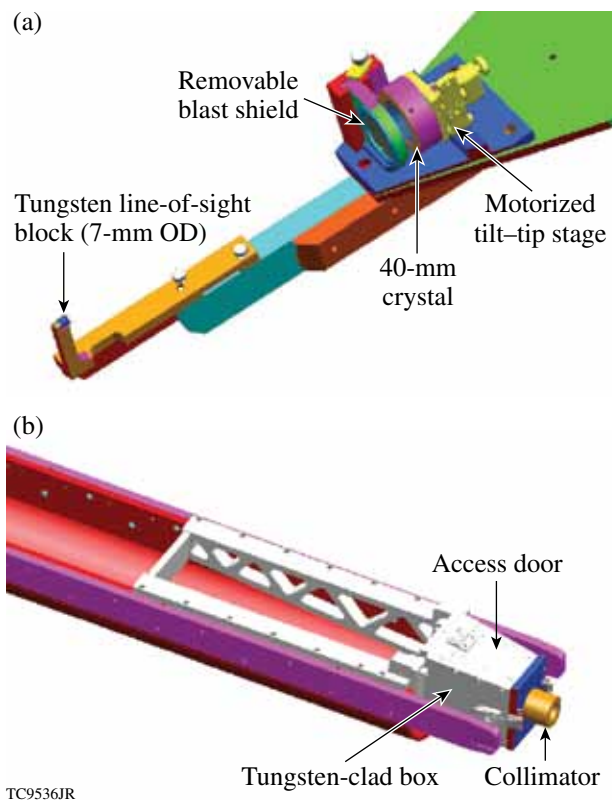


Figure 129.40

(a) CAD design of the crystal holder. The crystal is mounted on a motorized tip-tilt stage. A blast shield protects the crystal from target debris and can be removed for alignment. (b) CAD design of the image-plate holder. A tungsten-clad box houses the image plate, which records the image formed by the spherically bent crystal. An additional collimator is installed to further reduce the background from direct and Compton-scattered x rays. A filter foil is mounted in front of the collimator to optimize the signal level on the image-plate detector.

the crystal was sufficient for all experimental conditions. The blast-shield holder also accepts 1-mm-thick stainless-steel apertures to limit the active area of the crystal and to control the signal level on the detector. A 7.5-mm-thick, 7-mm-diam tungsten block protects the detector from x rays along the direct line of sight. The line-of-sight block is mounted on an arm attached to the crystal holder.

A CAD model of the image-plate detector's housing is shown in Fig. 129.40(b). A well-shielded, tungsten-clad box is mounted in the TIM opposing the crystal holder. An access door affords the operator easy access to insert the image-plate before the shot and remove it after the shot. A tungsten collimator reduces the field of view of the detector to suppress background from Compton scattering and fluorescence from structures in the target chamber. A Cu foil mounted in front of

the collimator acts as a K-edge filter¹⁴ to further improve the signal-to-background ratio. This filter is also used to optimize the signal level on the image-plate detector to prevent saturation. Typical filter thicknesses used in experiments range from 10 to 50 μm .

Alignment

The alignment procedure for the SCI system requires a number of steps. A pointer is first attached to the crystal holder hardware, and both the line-of-sight block and the blast shield are removed (Fig. 129.41). The tip of the pointer is optically aligned to target chamber center (TCC). The pointer is designed to set the distance from the crystal to the target to 276 mm, when the target is aligned to TCC. Mechanical alignment features in the pointer mount make a highly repeatable mounting of the pointer relative to the crystal mount possible. The pointer mount was designed not to block the two orthogonal lines of sight of the OMEGA EP Target Viewing and Alignment System. A precision of better than 100 μm can be achieved with this procedure.

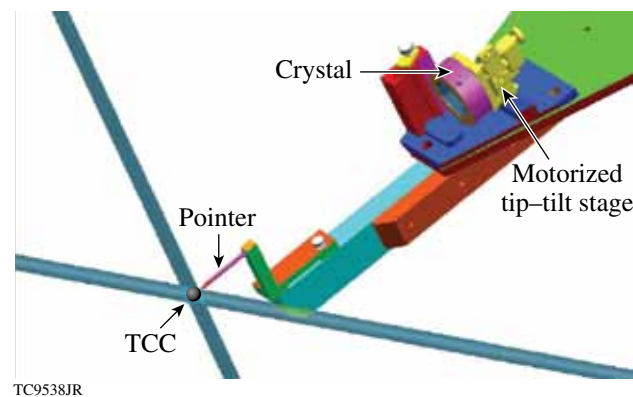


Figure 129.41

CAD design of the crystal holder in its pre-alignment configuration. A pointer is attached to the crystal holder hardware and optically aligned at target chamber center (TCC). The long, thin cylinders indicate the optical paths of the Target Viewing System.

In the next step the TIM coordinates are recorded, the TIM is retracted, and the pointer is removed from the crystal holder. The TIM is inserted again to its prerecorded position. Extensive tests have shown that this retract-and-insert cycle places the crystal back to the prerecorded position to within better than 100- μm accuracy. The tip of a single-mode fiber mounted in a third TIM is placed at TCC using the Target Viewing and Alignment System (Fig. 129.42). Light from an infrared (1053-nm) laser source is injected into the fiber. This light exits the fiber tip in an $\sim f/2$ cone toward the spherically

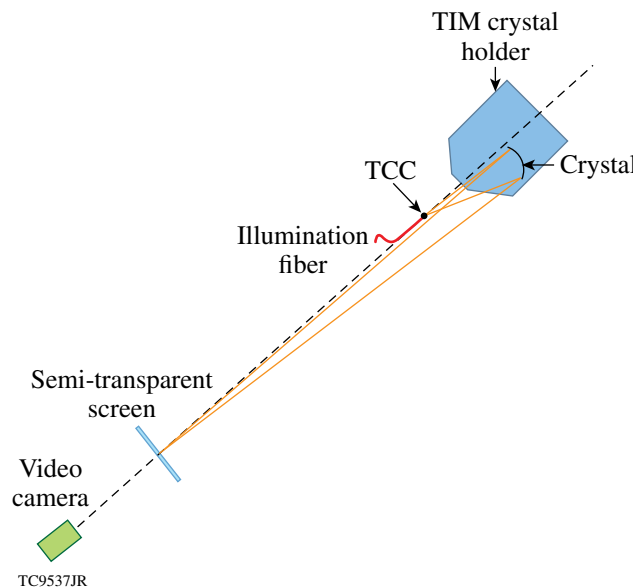


Figure 129.42

Schematic of the spherical crystal imager hardware in alignment mode. An illumination fiber is placed at TCC. Light from the fiber is reflected from the crystal to the semi-transparent screen. A video camera is used to optimize the focal spot on the screen.

bent crystal. A fraction of the infrared light is reflected off the crystal surface and sent toward the opposing TIM. The image-plate detector box in the opposing TIM is replaced by a semi-transparent screen, which is placed at the same distance from TCC as the image plate. This screen is viewed by an infrared-sensitive video camera. The motorized tip-tilt stages of the crystal mount are used to position the image formed by the spherical crystal at the center of the screen. Small corrections of the TIM insertion axis are used to optimize the focus of the crystal imager. The wavelength of the alignment source is not crucial. Off-line tests with a 680-nm-wavelength red laser have shown similar results. It is critical to use a single-mode fiber to generate a well-defined object, so that the crystal produces a clean image that can be used to optimize the focus.

Finally, the fiber is removed from its TIM, and the semi-transparent screen is replaced with the image-plate detector box. The crystal holder is retracted, and the blast shield and line-of-sight block are re-installed. The crystal holder is inserted again and the SCI system is ready for shots.

Experimental Data

Figure 129.43 shows one of the first images recorded with the SCI system. A $500 \times 500 \times 20\text{-}\mu\text{m}^3$ Cu foil was irradiated by an $\sim 1\text{-kJ}$, 10-ps OMEGA EP laser pulse. The SCI views the target from an angle of 63° relative to the target normal, which

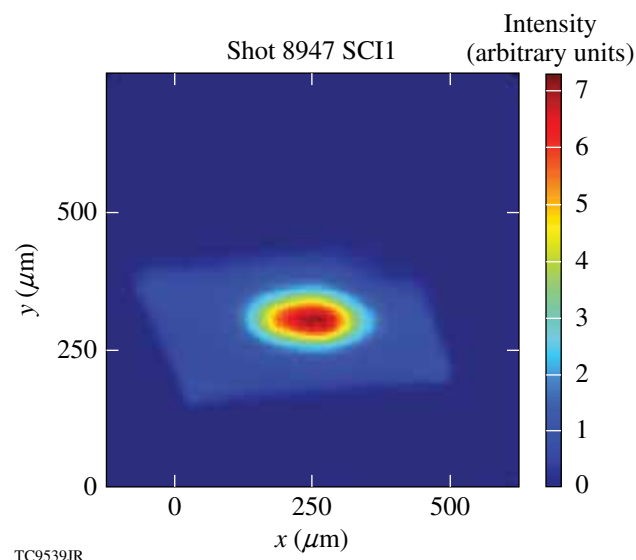


Figure 129.43

K_α image of a $500 \times 500 \times 20\text{-}\mu\text{m}^3$ Cu foil, irradiated by an $\sim 1\text{-kJ}$, 10-ps, $\sim 40\text{-}\mu\text{m}$ -diam OMEGA EP laser pulse. The spatial coordinates are scaled to the object plane.

leads to a foreshortening of the image in the vertical direction by a factor of ~ 2 . Even though the laser focal spot is only $\sim 40\text{ }\mu\text{m}$ in diameter, the image shows that the K_α radiation is emitted from the whole target area with an $\sim 100\text{-}\mu\text{m}$ -diam bright spot located roughly where the laser hits the target. This image is consistent with other observations that show that most of the electrons generated in the laser–plasma interactions are confined to the target by strong electric fields set up when the first high-energy electrons leave the target and charge it to a multi-MeV potential.^{15–17} The confined electrons flood the target and generate a quasi-uniform emission. The slightly darker area on the top-right corner of the target is due to the fact that the target is attached to a stalk at this corner, which allows the electrons to escape, thereby reducing the K_α emission.

The signal-to-background ratio is evaluated by measuring the average value of the signal on the image plate outside the object and comparing it to the signal measured at the edge of the image and the peak in the center of the image. With a typical background signal of 0.01 photostimulated luminescence (PSL) outside the image, ~ 1 PSL at the edge, and ~ 6 PSL at the peak, signal-to-background levels of 100 to 600 are observed.

To assess the spatial resolution of the SCI, lineouts are taken across the edge of the image at different locations (see Fig. 129.44). The rise of the signal from 10% to 90% of its

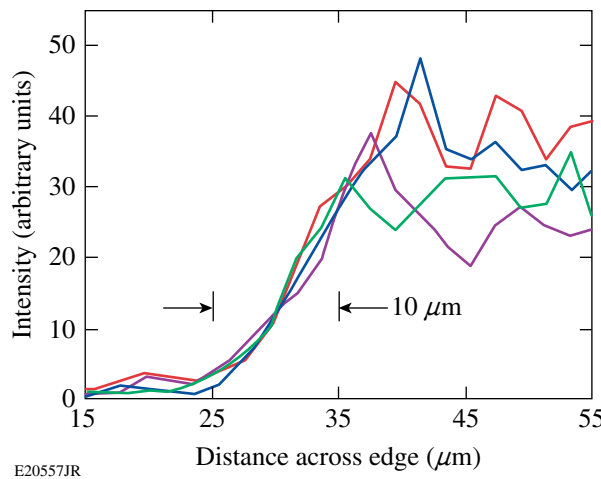


Figure 129.44

Edge lineouts of an image from the SCI at different locations. The signal rises from 10% to 90% of the peak in $\sim 10 \mu\text{m}$ for the locations where the imager is in best focus.

peak value is taken as a figure of merit for the resolution of the imaging system. This 10% to 90% criterion is a more-stringent measure of resolution, compared to a measurement of the modulation transfer function, where the resolution is usually defined at either a 50% or 10% contrast value. Since the imager has a limited depth of focus and views the object from a steep angle of 63° relative to the target normal, the resolution changes across the edge from $\sim 10 \mu\text{m}$, where the object is in best focus, to $\sim 15 \mu\text{m}$ outside best focus.

A series of experiments were performed to measure the depth of focus of the imaging system by intentionally changing the crystal's distance from the target from the optimal position as determined by the pre-shot optical alignment (see Fig. 129.45). The best resolution of the SCI is observed in these experiments for displacements of $<100 \mu\text{m}$ from the pre-shot alignment. At larger displacements the resolution deteriorates to values of the order of $20 \mu\text{m}$ at $300\text{-}\mu\text{m}$ displacement.

Summary and Conclusions

A crystal imaging system that can be fully remotely aligned has been implemented on OMEGA EP. A spherically bent quartz crystal is used to image the Cu K_α emission of targets irradiated with up to 1 kJ of laser energy at a 10-ps pulse duration. Experiments performed to map out the depth of focus of the crystal imager showed that the pre-shot optical alignment sets the SCI to its optimum focus condition. A best-focus resolution of $\sim 10 \mu\text{m}$, measured as the 10% to 90% rise on the edge of the image, has been achieved. The images show a very high signal-to-background ratio of >100 , which indicates that the

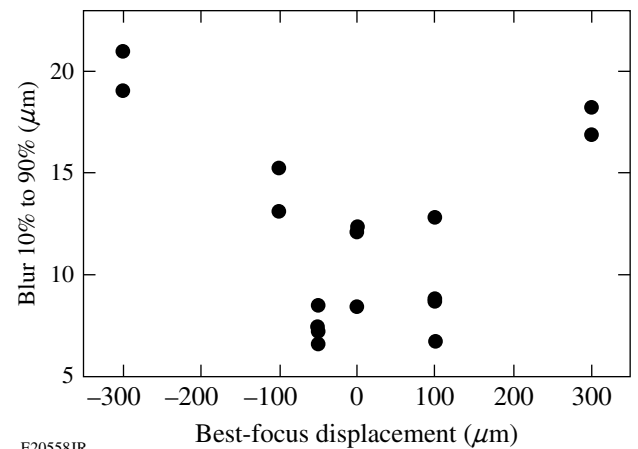


Figure 129.45

Edge rise from 10% to 90% of the peak as a function of defocus in the spherical crystal imager. Zero displacements are defined as the locations of the pre-shot optical alignment.

shielding concepts used in the setup of the SCI are effective and will provide adequate shielding even at the highest planned energies of 2.6 kJ at 10 ps on OMEGA EP. A similar crystal imaging system has been implemented on the OMEGA Laser System. Only minor adjustments to the mechanical layout of this system are required to adapt it to other spectral lines using different crystals and Bragg angles. Designs to modify the SCI to image the Si He_α spectral line are currently underway.

ACKNOWLEDGMENT

This work was supported by the U.S. Department of Energy Office of Inertial Confinement Fusion under Cooperative Agreement No. DE-FC52-08NA28302, the University of Rochester, and the New York State Energy Research and Development Authority. The support of DOE does not constitute an endorsement by DOE of the views expressed in this article.

REFERENCES

1. T. A. Pikuz *et al.*, in *EUV, X-Ray, and Neutron Optics and Sources*, edited by C. A. MacDonald *et al.* (SPIE, Bellingham, WA, 1999), Vol. 3767, pp. 67–78.
2. Y. Aglitskiy *et al.*, *Appl. Opt.* **37**, 5253 (1998).
3. J. A. Koch *et al.*, *Rev. Sci. Instrum.* **74**, 2130 (2003).
4. T. Missalla *et al.*, *Rev. Sci. Instrum.* **70**, 1288 (1999).
5. Ch. Reich *et al.*, *Phys. Rev. E* **68**, 056408 (2003).
6. S. Le Pape *et al.*, *Rev. Sci. Instrum.* **79**, 106104 (2008).
7. J. A. King, K. Akli, R. A. Snavely, B. Zhang, M. H. Key, C. D. Chen, M. Chen, S. P. Hatchett, J. A. Koch, A. J. MacKinnon, P. K. Patel,

-
- T. Phillips, R. P. J. Town, R. R. Freeman, M. Borghesi, L. Romagnani, M. Zepf, T. Cowan, R. Stephens, K. L. Lancaster, C. D. Murphy, P. Norreys, and C. Stoeckl, Rev. Sci. Instrum. **76**, 076102 (2005).
8. L. J. Waxer, D. N. Maywar, J. H. Kelly, T. J. Kessler, B. E. Kruschwitz, S. J. Loucks, R. L. McCrory, D. D. Meyerhofer, S. F. B. Morse, C. Stoeckl, and J. D. Zuegel, Opt. Photonics News **16**, 30 (2005).
9. C. Stoeckl, J. A. Delettrez, J. H. Kelly, T. J. Kessler, B. E. Kruschwitz, S. J. Loucks, R. L. McCrory, D. D. Meyerhofer, D. N. Maywar, S. F. B. Morse, J. Myatt, A. L. Rigatti, L. J. Waxer, J. D. Zuegel, and R. B. Stephens, Fusion Sci. Technol. **49**, 367 (2006).
10. K. Fujita *et al.*, Rev. Sci. Instrum. **72**, 744 (2001).
11. Photonics Products Group, Inc., Northvale, NJ 07647.
12. A. L. Meadowcroft, C. D. Bentley, and E. N. Stott, Rev. Sci. Instrum. **79**, 113102 (2008).
13. New Focus, Inc., A Division of Newport Corporation, Irvine, CA 92606.
14. C. Stoeckl, W. Theobald, T. C. Sangster, M. H. Key, P. Patel, B. B. Zhang, R. Clarke, S. Karsch, and P. Norreys, Rev. Sci. Instrum. **75**, 3705 (2004).
15. J. Myatt, W. Theobald, J. A. Delettrez, C. Stoeckl, M. Storm, T. C. Sangster, A. V. Maximov, and R. W. Short, Phys. Plasmas **14**, 056301 (2007).
16. P. M. Nilson, W. Theobald, J. Myatt, C. Stoeckl, M. Storm, O. V. Gotchev, J. D. Zuegel, R. Betti, D. D. Meyerhofer, and T. C. Sangster, Phys. Plasmas **15**, 056308 (2008).
17. K. U. Akli, M. H. Key, H. K. Chung, S. B. Hansen, R. R. Freeman, M. H. Chen, G. Gregori, S. Hatchett, D. Hey, N. Izumi, J. King, J. Kuba, P. Norreys, A. J. Mackinnon, C. D. Murphy, R. Snavely, R. B. Stephens, C. Stoeckel, W. Theobald, and B. Zhang, Phys. Plasmas **14**, 023102 (2007).